Int J Adv Manuf Technol (2006) 29: 637–647
DOI 10.1007/s00170-005-2572-6

ORIGINAL ARTICLE

M. Wan · W.H. Zhang

Calculations of chip thickness and cutting forces in flexible end milling

Received: 10 November 2004 / Accepted: 15 January 2005 / Published online: 12 October 2005

Abstract In the end milling process of a flexible workpiece, it is well recognized that the precise determination of the instantaneous uncut chip thickness (IUCT) is essential for the cutting force calculation. This paper will present a general method that incorporates simultaneously the cutter/workpiece deflections and the immersion angle variation into the calculation of the IUCT and cutting forces. Contributions are twofold. Firstly, considering the regeneration model, a new scheme for the IUCT calculation is determined based on the relative positions between two adjacent tooth path centers. Secondly, a general approach is established to perform numerical validations. On one hand, the engagement/separation of the cutter from the workpiece is instantaneously identified. On the other hand, the calculation of the IUCT is iteratively performed. To demonstrate the validity of the method, several examples are used to show the convergence history of the cutting force and the IUCT during the flexible end milling process. Both theoretical analyses and numerical results show that the regeneration mechanism is short lived and will disappear after several tooth periods in flexible static end milling process.

Keywords Chip thickness · Cutting forces · End milling · Radial depth of cut

1 Introduction

End milling is a widely used manufacturing process in aerospace, automobile, and die-mold industries for slotting and shaping thin-walled workpieces. With the advancement of CAD/CAM technologies, more and more parts such as the aircraft wing panels, engine blades are milled by removing extra material from monolithic blanks. However, the increased complexity of parts and the extreme properties of machining materials are continuing to challenge the current manufacturing capability. To obtain productivity improvement and required machining quality, reliable machining technologies must be employed. One of the efficient ways is to simulate the critical milling attributes such as machinability, surface quality, cutter wear/fracture, and chatter [1–10] and then some machining planning and online monitoring methods will be figured out. It is recognized that the modeling of cutting forces constitutes the basis for all simulation work. To this end, an earlier fundamental of milling kinematics was analyzed by Martellotti [11], who pointed out that the trochoidal path of each milling tooth could be approximated by a circular path at each tooth-passing interval. Koenigsberger et al. [12] proposed that the cutting forces are proportional to the IUCT and the proportional coefficients, i.e., cutting coefficients may be assumed to be constants with respect to the average chip thickness. With this idea in mind, Kline et al. [13] presented a numerical model for the prediction of cutting forces in end milling. Considering the chip thickness variation, a more accurate prediction scheme using the cutting coefficients as exponential functions of the average uncut chip thickness was proposed by Altintas et al. [14]. In all the above models, it is necessary to note that combining effects of the shearing mechanism on the rake face together with the rubbing or ploughing mechanism at the cutting edge are reflected by a single coefficient. By separating these two mechanisms, Budak et al. [15] used the measured cutting forces and orthogonal cutting data, respectively, to calibrate two such independent coefficients. For the same purpose, an on-line method was also proposed by Zheng et al. [16]. Besides, Armarego et al. [17] proposed a cutting force prediction model by transforming orthogonal cutting parameters to oblique milling ones. Yücesan's model [18] accounted for the effects of the friction, pressure as well as the force flow angle.

Clearly, all cutting force models mentioned above are based on the local cutting analysis and rely on the IUCT. In fact, the cutter/workpiece deflections affect the IUCT in the highly flexible cutting process. To understand effects of cutting parameters upon the IUCT and also effects of the latter on the cutting forces, investigations have been made on the calculation of the IUCT in

M. Wan · W.H. Zhang (✉)
Sino-French Laboratory of Concurrent Engineering,
Department of Aircraft Manufacturing Engineering,
Northwestern Polytechnical University, P.O. Box 552,
710072 Xi'an, Shaanxi, China
E-mail: zhangwh@nwpu.edu.cn
Tel.: +86-29-88495774

terms of the runout and deflections. Sutherland et al. [19] proposed a regeneration model to calculate the IUCT by considering both the runout and the cutter's deflection. Kline et al. [20] evaluated the IUCT by accounting for the parallel axis offset cutter runout with negligence of workpiece/cutter deflections. Smith et al. [21] also suggested a geometric progression regeneration model to predict the IUCT. Later, an iterative formulation that relates the cutting forces in the current tooth period to those in the previous tooth period was proposed by Budak et al. [1], who considered the effect of cutter defections upon the IUCT and the cutting forces, but didn't take into account the influence of workpiece deflections and the immersion angle variation. Their numerical results showed that the cutting forces deduced from the regeneration model converge to those produced by using nominal chip thickness values in few tooth intervals.

This paper presents a general method for the prediction of the IUCT and cutting forces. The prominent feature of this method is that it incorporates the effects of the cutter/workpiece deflections and the immersion angle variation. A new IUCT computing scheme is proposed according to the IUCT definition. In particular, an improved iterative algorithm is presented to correct the IUCT and the radial depth of cut. The algorithm uses the concept of correction factor or weighted parameter to ensure the convergence. In addition to these, two typical cutting force models are used to study the regeneration model. By using numerical tests of flexible static end milling process, it concludes that the regeneration phenomena always disappear after several tooth periods. This conclusion ensures that the nominal uncut chip thickness can be used reliably for all simulation work of the static end milling process.

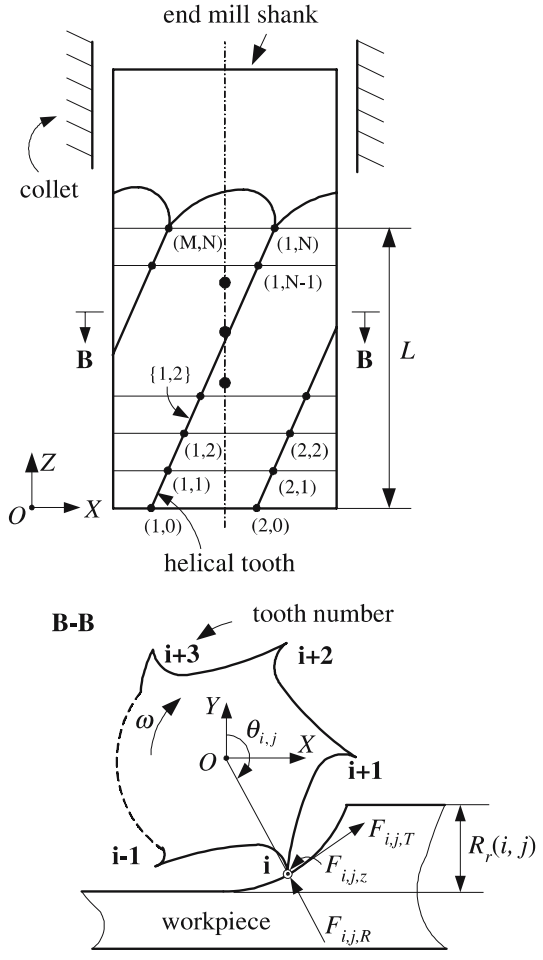

Fig. 1. Cutter's model in down milling

2 Basic mechanistic model of end milling

2.1 Modeling of the cutter and the workpiece

The end milling process is simulated by means of the finite element method. To simplify the modeling procedure, a great flexibility is offered to users who are able to discretize the cutter and the workpiece independently, i.e., coordinate systems, meshing methods and element types are selected independently according to their own structural characteristics. In this study, the helical end mill is axially divided into N elements of equal length along the cutter axis as shown in Fig. 1. Here, notation (i, j) denotes the cutter node which is the intersection between one horizontal mesh line and the ith cutting edge, while $\{i, j\}$ represents the cutter element which is the cutting edge segment between cutter node (i, j) and cutter node $(i, j+1)$. With the aid of any available finite element mesh generator, the workpiece may be discretized into a 3D irregular finite element mesh consisting of tetrahedral elements, prismatic elements, hexahedral elements or a combination of them.

2.2 Cutting force models

In this study, two popular cutting force models are considered to reveal the effects of the IUCT. By convention, $F_{i,j,T}$, $F_{i,j,R}$, $F_{i,j,z}$ denote the instantaneous tangential, radial and axial cutting forces acting on cutter element $\{i, j\}$.

- Model 1 [1, 4, 5, 14]

$$\begin{cases} F_{i,j,T} = K_T \cdot h_{i,j} \cdot dz \\ F_{i,j,R} = K_R \cdot F_{i,j,T} \\ F_{i,j,z} = K_z \cdot F_{i,j,T} \end{cases} \tag{1}$$

where $h_{i,j}$ and dz denote the IUCT and nominal axial length of cutter element $\{i, j\}$, respectively, with $dz = L/N$. $h_{i,j}$ measured in unit of length whose value depends upon the feed per tooth and the tooth path. The calculation of $h_{i,j}$ will be developed in Sect. 2.3. K_T, K_R and K_z are experimentally calibrated cutting coefficients, that combine the shearing mechanism at the shear zone with the rubbing or ploughing mechanism at the cutting edge. These coefficients can be treated as constants or power functions of the average uncut chip thickness $\bar{h}$.

$$K_T = k_T \bar{h}^{-k_p};\ K_R = k_R \bar{h}^{-k_q};\ K_z = k_z \bar{h}^{-k_a} \tag{2}$$

with k_T, k_R, k_z, k_p, k_q and k_a being determined from experiments.

- Model 2 [7, 15, 16]

$$\begin{cases} F_{i,j,T} = K_{Tc} \cdot h_{i,j} \cdot dz + K_{Te} \cdot dz \\ F_{i,j,R} = K_{Rc} \cdot h_{i,j} \cdot dz + K_{Re} \cdot dz \\ F_{i,j,z} = K_{zc} \cdot h_{i,j} \cdot dz + K_{ze} \cdot dz \end{cases} \tag{3}$$

where definitions of $h_{i,j}$ and dz are the same as in Model 1. K_{Tc}, K_{Rc}, K_{zc} are tangential, radial, and axial cutting force coefficients related to shearing, while K_{Te}, K_{Re}, K_{ze} are tangential, radial, and axial edge force coefficients related to rubbing or ploughing.

For each cutter element $\{i, j\}$, the instantaneous cutting forces may be expressed in XYZ coordinate system

$$\begin{cases} F_{i,j,X} = -F_{i,j,T} \cos\theta_{i,j} - F_{i,j,R} \sin\theta_{i,j} \\ F_{i,j,Y} = F_{i,j,T} \sin\theta_{i,j} - F_{i,j,R} \cos\theta_{i,j} \\ F_{i,j,Z} = F_{i,j,z} \end{cases} \tag{4}$$

where $\theta_{i,j}$ is the angle determined clockwise from the exterior normal of the machined workpiece to the cutting position of cutter element $\{i, j\}$. Since each cutter element is relatively small, the related cutting position is approximately assumed to be the middle point of cutter element $\{i, j\}$ without considering the variation of the helical angle in each element.

The resultant cutting forces F_X, F_Y, and F_Z acting on the whole cutter can be obtained by summing $F_{i,j,X}$, $F_{i,j,Y}$, and $F_{i,j,Z}$ over all cutter elements

$$F_X = \sum_{i,j} F_{i,j,X}, \; F_Y = \sum_{i,j} F_{i,j,Y}, \; F_Z = \sum_{i,j} F_{i,j,Z}\,. \tag{5}$$

However, for some cutter elements, one of two extreme cutter nodes may be disengaged from the workpiece while the other one is in cut. As depicted in Fig. 2, cutter node (i, j) is not in contact with the workpiece but cutter node $(i, j+1)$ is in contact with the workpiece. Therefore, the axial length of cutter element $\{i, j\}$ involved in Eqs. 1 and 3 has to be corrected based on the following relation

$$dz' = u_{i,j} dz \tag{6}$$

where $u_{i,j}$ is a correction factor of cutter element $\{i, j\}$ defined as

$$u_{i,j} = \frac{z_{i,j}}{dz} \tag{7}$$

where $z_{i,j}$ is the axial length of cutter element $\{i, j\}$ being in contact. For example, the correction factor of cutter element $\{i, j\}$ in Fig. 2 equals $\overline{EC}/\overline{ED}$.

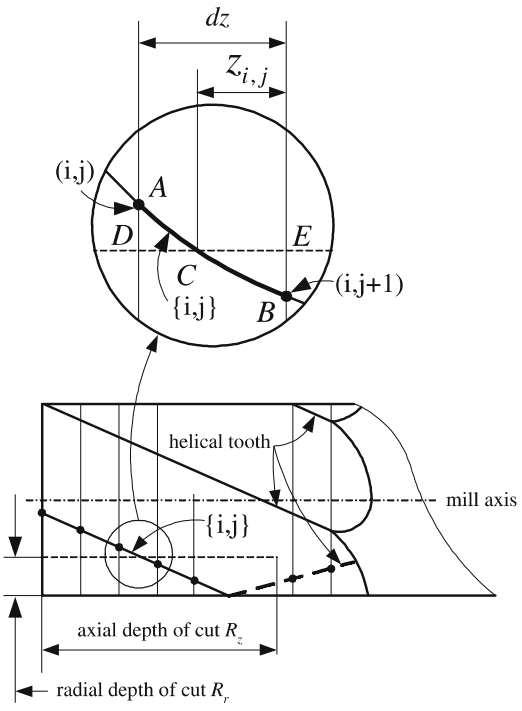

Fig. 2. Illustrations of correction factor in up milling

2.3 Calculation of the IUCT

As illustrated in Fig. 3, at an instantaneous cutting position of cutter element $\{i, j\}$, the IUCT, $h_{i,j}$, refers to the distance in the radial direction of the cutter between the tooth path to be generated by the cutter element $\{i, j\}$ and the surface left by the previous cutter element $\{i-m, j\}$. Note that $m \neq 1$ implies

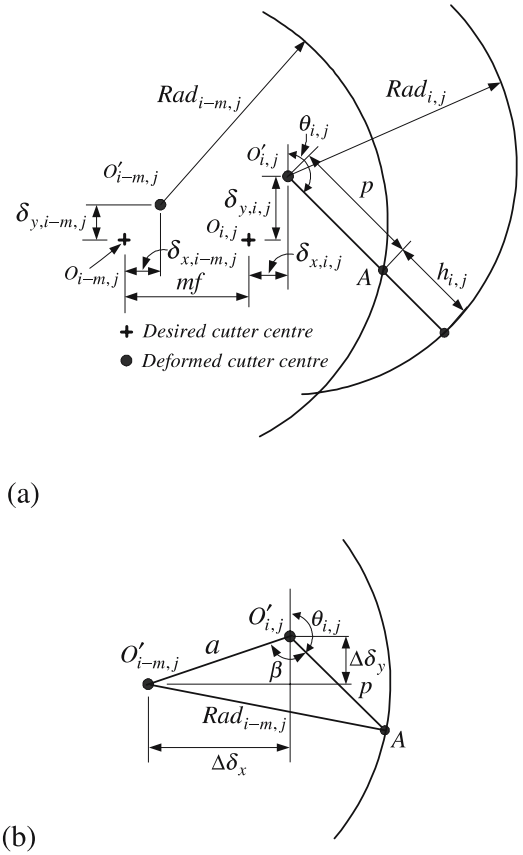

Fig. 3a,b. Geometric illustration of chip thickness **a** Definition of the IUCT **b** Geometric relation for the regeneration model

the existence of runout. Due to the deflections of the cutter and workpiece, the cutter axis shifts from its nominal position. As a result, two adjacent tooth paths will deviate from the desired paths. So, $h_{i,j}$ will be different from the nominal values. Based on the circular tooth path assumption [11] shown in Fig. 3a, $h_{i,j}$ is calculated as follows

$$h_{i,j} = Rad_{i,j} - p \tag{8}$$

where $Rad_{i,j}$ is the radius of the circular tooth path to be generated by cutter element $\{i, j\}$ and p is an intermediate variable shown in Fig. 3.

Using the law of cosines, a geometry relation exists between the cutter center of the current tooth path and that of the past tooth path in Fig. 3b.

$$Rad_{i-m,j}^2 = a^2 + p^2 - 2ap\cos\beta \tag{9a}$$

in which

$$a = \sqrt{\Delta\delta_x^2 + \Delta\delta_y^2} \tag{9b}$$

with

$$\Delta\delta_x = m f + \delta_{x,i,j} - \delta_{x,i-m,j}, \quad \Delta\delta_y = \delta_{y,i,j} - \delta_{y,i-m,j} \tag{9c}$$

$(\delta_{x,i,j}, \delta_{y,i,j})$, and $(\delta_{x,i-m,j}, \delta_{y,i-m,j})$ correspond to offset values of cutter centers of the current tooth and the m-past tooth from their desired positions, respectively. f is the feed per tooth. Obviously,

$$\beta = \pi - \theta_{i,j} + \arccos\left(\frac{\Delta\delta_y}{a}\right). \tag{10}$$

By solving Eq. 9a, p is obtained as

$$p = a\cos\beta + \sqrt{Rad_{i-m,j}^2 - a^2\sin^2\beta}. \tag{11}$$

By substituting Eq. 11 into Eq. 8, $h_{i,j}$ is derived as

$$h_{i,j} = -a\cos\beta + Rad_{i,j} - \sqrt{Rad_{i-m,j}^2 - a^2\sin^2\beta}. \tag{12}$$

Due to the fact that $Rad_{i-m,j} \gg \Delta\delta_x$ and $Rad_{i-m,j} \gg \Delta\delta_y$, it follows that $Rad_{i,k-m} \gg a\sin\beta$ from Eq. 9b. Thus, Eq. 12 can be approximated by

$$h_{i,j} = -a\cos\beta + Rad_{i,j} - Rad_{i-m,j}. \tag{13}$$

Note that if a negative value of $h_{i,j}$ is obtained by Eq. 12 or Eq. 13, $h_{i,j}$ is set to be zero.

Physically, a static milling process free of vibration implies that cutting forces have surely stabilized themselves after a few tooth periods. In other words, cutting forces obtained from two adjacent tooth periods must be equal, as assumed by Budak [1]. The implication of this stability condition requires that the volume of materials cut off by the current tooth should be identical to that cut off by the previous tooth with the negligence of runout, i.e., $m = 1$ and $Rad_{i,j} = Rad_{i-1,j}$ in Eq. 13. Now, suppose that $F_i(\theta_{i,j})$ represents the resultant cutting force vector associated with the cutter position angle $\theta_{i,j}$, then

$$F_i(\theta_{i,j}) = F_{i-1}(\theta_{i-1,j}). \tag{14}$$

Likewise, cutter deflections of the concerned cutter segment also remain unchanged between two adjacent teeth so that the following equations hold

$$\delta_{i,j}^t = \delta_{i-1,j}^t \tag{15}$$

where $\delta_{i,j}^t = (\delta_{i,j}^{t,X}, \delta_{i,j}^{t,Y}, \delta_{i,j}^{t,Z})$ is the cutter deflection vector corresponding to the cutter element $\{i, j\}$. It is evaluated based on the cantilevered beam model [4, 7, 19].

Concerning the cutter center offset values $(\delta_{x,i,j}, \delta_{y,i,j}, \delta_{x,i-1,j}, \delta_{y,i-1,j})$, because of $\delta_{x,i,j} = \delta_{i,j}^{t,X}$ and $\delta_{y,i,j} = \delta_{i,j}^{t,Y}$, the following important relations can be derived.

- From Eq. 15,

$$\delta_{x,i,j} = \delta_{x,i-1,j}, \quad \delta_{y,i,j} = \delta_{y,i-1,j} \tag{16a}$$

- From Eq. 9c,

$$\Delta\delta_x = f, \quad \Delta\delta_y = 0 \tag{16b}$$

- From Eq. 10,

$$\beta = \frac{3\pi}{2} - \theta_{i,j} \tag{16c}$$

By reviewing the above relations, Eq. 13 can be further simplified as

$$h_{i,j} = f\sin\theta_{i,j}. \tag{17}$$

Obviously, Eq. 17 indicates that $h_{i,j}$ converges to its nominal value of $f\sin\theta_{i,j}$ in a static milling process. This conclusion deduced from the basic definition of IUCT agrees completely with that from the forces-based iterative equation by Budak [1] although both formulations are different.

3 Deflection-based adaptive algorithms for the convergence of chip thickness and radial depth of cut

3.1 Basic iterative scheme for the evaluation of chip thickness and radial depth of cut

As shown in Fig. 4, if the cutter/workpiece deflections are negligible, AB is the ideal contact curve of the cutting tooth. However, due to the cutter/workpiece deflections, the nominal intersection line DF between the cutter and the workpiece will be transformed into curve EH. As a result, for any cutter node (i, j) in cut, nominal values of radial depth of cut $R_r(i, j)$, immersion angle $\varphi_{i,j}$, and the chip thickness $h_{i,j}$ will be influenced. To

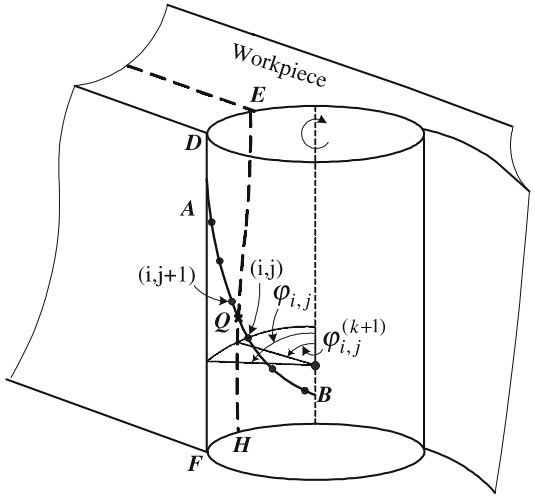

Fig. 4. Illustration of immersion angle

predict actual values of $R_r(i, j)$ and $h_{i,j}$, a numerical adaptive algorithm is develop based on deflections ($\delta_{i,j}^{t,Y}$, $\delta_{i,j}^{w,Y}$). Here, $\delta_{i,j}^{w,Y}$ is the normal deflection of the workpiece corresponding to the cutter node (i, j). It is evaluated here by elastic FEA using the unit load method.

In a specified cutter angular position, $R_r(i, j)$ can be iteratively corrected by

$$R_r^{(k+1)}(i, j) = R_r(i, j) - \left[\delta_{i,j}^{t,Y\,(k)} + \delta_{i,j}^{w,Y\,(k)}\right] \quad k = 0, 1, \cdots, n$$

s.t.

$$\left|R_r^{(k+1)}(i, j) - R_r^{(k)}(i, j)\right| < \varepsilon \tag{18}$$

where $R_r^{(k+1)}(i, j)$ is the corrected radial depth of cut in the $(k+1)$th iteration. $R_r(i, j)$ is the known nominal value. $\delta_{i,j}^{t,Y\,(k)}$ and $\delta_{i,j}^{w,Y\,(k)}$ denote normal deflections of cutter node (i, j) and of the workpiece in the kth iteration, respectively.

Furthermore, it can be seen from Fig. 4 that the immersion angle of an arbitrary cutter node (i, j) changes from its nominal value $\varphi_{i,j}$ to $\varphi_{i,j}^{(k+1)}$. The latter can be evaluated in terms of $R_r^{(k+1)}(i, j)$ by

$$\varphi_{i,j}^{(k+1)} = \arccos\left(1 - \frac{R_r^{(k+1)}(i, j)}{Rad_{i,j}}\right). \tag{19}$$

Due to the variation of the immersion angles, the contact curve AB of the cutting tooth will be shortened to QB (see Fig. 4). Consequently, some cutter nodes may be out of cut, e.g., cutter node $(i, j+1)$ and a certain number of cutter elements that should be completely in contact may now become partially engaged, e.g., cutter element $\{i, j\}$. With the aid of Eq. 19, the status of each cutter node can be properly identified. For cutter node (i, j), if $\pi - \psi_{i,j} \le \varphi_{i,j}^{(k+1)}$, cutter node (i, j) is in cut. Otherwise, it is out of cut. Here, $\psi_{i,j}$ designates the angle determined clockwise from the positive direction of axis Y to the cutter node (i, j). In Fig. 4, cutter element $\{i, j\}$ is partially in cut, the actual contact length $z_{i,j}^{(k+1)}$ can be obtained as follows

$$z_{i,j}^{(k+1)} = \frac{\left(\varphi_{i,j}^{(k+1)} + \psi_{i,j} - \pi\right) \cdot D \cdot \mathrm{ctg}\,\gamma}{2} \tag{20}$$

where γ and D represent the helix angle and the diameter of the cutter, respectively.

Besides, the chip thickness has to be iterated as follows

$$h_{i,j}^{(k+1)} = -a^{(k)} \cos\beta^{(k)} + Rad_{i,j} - Rad_{i-m,j} \tag{21}$$

where $a^{(k)}$ and $\beta^{(k)}$ will be updated according to equations given in Sect. 2.3 for every new pair of cutter/workpiece deflections.

3.2 Sub-iteration algorithm for the determination of chip thickness and radial depth of cut

During the iterative process of Eqs. 18 and 21, the variation of both radial cutting depth and chip thickness is found to be very sensible so that numerical oscillations may occur. To avoid the divergence, following sub-iteration algorithms are adopted.

- A relatively small change of the chip thickness is used

$$\tilde{h}_{i,j}^{(k+1)} = \lambda \cdot (h_{i,j}^{(k+1)} - \tilde{h}_{i,j}^{(k)}) + \tilde{h}_{i,j}^{(k)} \quad 0 < \lambda \le 1 \tag{22}$$

  where $\tilde{h}_{i,j}^{(k+1)}$ is the corrected value of the instantaneous uncut chip thickness for cutting force calculation in the $(k+1)$th iteration. $h_{i,j}^{(k+1)}$ is the value of the instantaneous uncut chip thickness obtained from Eq. 21. λ is the weighted parameter given a priori.
- The oscillation of radial depth of cut is prevented as follows

  Case 1 Single cutter element in oscillation. As shown in Fig. 5, suppose that the cutter element $\{i, j\}$ is engaged partially in contact with the workpiece. Because cutter/workpiece deflections lead to a relatively large variation of radial depth of cut $R_r^{(k)}(i, j)$, the correction factor $u_{i,j}$ defined in Eq. 7 may be divergent as illustrated in Fig. 6. To solve this problem, a sub-iterative scheme is first adopted to stabilize $u_{i,j}$.

$$\tilde{u}_{i,j}^{(k+1)} = \xi \cdot (u_{i,j}^{(k+1)} - \tilde{u}_{i,j}^{(k)}) + \tilde{u}_{i,j}^{(k)}$$

$$u_{i,j}^{(k+1)} = \frac{z_{i,j}^{(k+1)}}{dz} \quad k = 0, 1, \cdots, n$$

s.t.

$$0 < \xi \le 1$$

$$\left|\tilde{u}_{i,j}^{(k+1)} - u_{i,j}^{(k+1)}\right| \le \varepsilon \tag{23}$$

  where $\tilde{u}_{i,j}^{(k+1)}$ is the corrected value of the correction factor for cutting force calculation in the $(k+1)$th iteration. $u_{i,j}^{(k+1)}$ and $z_{i,j}^{(k+1)}$ are the actual values of the correction factor and the axial contacting length related to cutter element $\{i, j\}$, respectively. ξ is the weighted parameter given a priori.

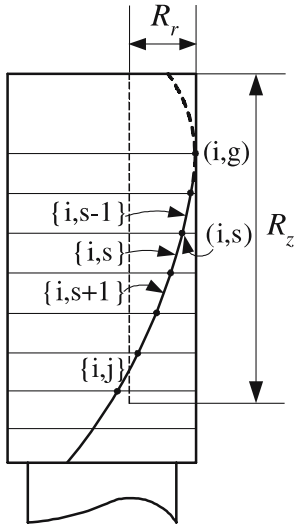

Fig. 5. Illustration of partially engaged cutter elements

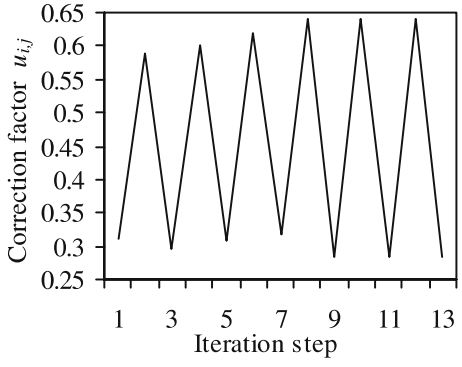

Fig. 6. Oscillation of a single correction factor $u_{i,j}$

Case 2 Multiple cutter elements in oscillation. Some cutter elements, e.g., $\{i, s\}, \{i, s+1\}, \ldots, \{i, j\}$ shown in Fig. 5, may also be engaged in cut in the current iteration and disengaged in the next one. In this case, the following procedure is proposed to ensure the convergence of the iteration scheme.

(a). Assume that cutter elements from $\{i, s+1\}$ to $\{i, j\}$ are not engaged in cut. So, set $R_r^{(k)}(i,t) = 0$ for all $(s+1 \le t \le j)$.

(b). Start the iterative process of Eqs. 22 and 23 for the cutter element $\{i, s\}$ with $\tilde{u}_{i,s}^{(k+1)}$ until the convergence is reached.

(c). If $0 \le \tilde{u}_{i,s}^{(k+1)} < 1$, the convergence achieves for all cutter elements and stop the iteration. Otherwise, continue step (b) by setting $s = s+1$ and $R_r^{(k)}(i,s) = R_r^{(k)}(i,s-1)$.

After $\tilde{u}_{i,s}^{(k+1)}$ is updated, the axial depth of cut will be corrected correspondingly. Note that Case 1 and Case 2 discussed above correspond to the down milling process. In the up milling process, Case 1 is still applicable. Instead, the oscillation will happen for cutter elements near the cutter tip in Case 2. Therefore, oscillating cutter elements, e.g., $\{i, s\}, \{i, s-1\}, \ldots, \{i, j\}$ are needed to be identified sequentially as performed in down milling.

3.3 The whole simulation procedure

As shown in Fig. 7, the solution procedure consisting of basic algorithms presented above is summarized for a specified cutter rotation angular step. Since uncut chip thickness has relations with two adjacent tooth periods, cutter/workpiece deflections should be initialized firstly. Initial values can be either set to zero or values calculated by the correction algorithms of the radial depth of cut using the nominal chip thickness.

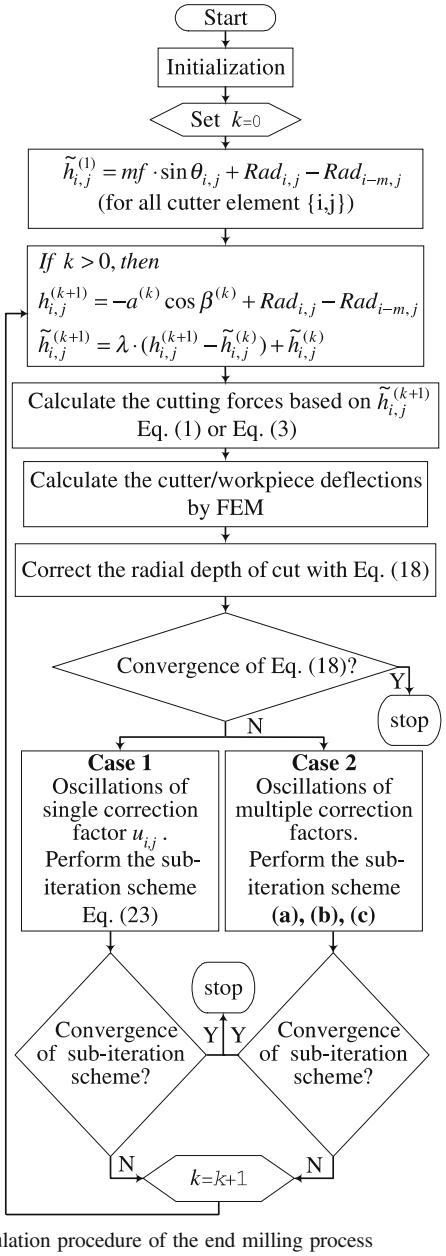

Fig. 7. Simulation procedure of the end milling process

4 Numerical applications

To check the validity of the proposed algorithm in predicting the uncut chip thickness and the cutting forces, four numerical tests are carried out for the workpiece shown in Fig. 8. For Test 1, Test 2, and Test 4, the machined surface is meshed with 50×40 elements; whereas in Test 3, the machined surface is discretized with 70×40 elements. For all tests, corresponding results are compared with those found in literature. Cutting parameters such as cutting force model, cutting force coefficients, axial and radial depths of cut, geometrical characteristics of the cutter and workpiece are all listed in Table 1.

Test 1: Based on the cutting force Model 1, a comparison is made between the cutting forces obtained with nominal chip thickness and iteration chip thickness, respectively. In both cases, the radial depth of cut is iteratively updated. Figure 9a gives the convergence history of the chip thickness associated with cutter element {1,35} versus cutter angular position during the milling process. The iteration value converges very quickly to the nominal value after several rotation angles. In detail, Figs. 9b and c show the sub-iteration histories of the chip thickness in the 2nd and the 8th tooth periods with $\theta_{1,35} = 166.684°$, respectively. From the profiles, we can see that after the convergence is achieved, deviations between nominal values and iteration values are relatively large in the 2nd tooth period, but deviations are approximately zeros in the 8th period. This is because the cutting steady state has not yet been attained in the former. In Fig. 10a, resultant cutting forces have been predicted. It turns out that the cutting forces based on the iterated chip thickness converge toward those using nominal chip thickness both in magnitude and in profile after few tooth periods. For the purpose of comparison, referenced results of [5] are shown in Fig. 10b, that confirm the correctness of current solutions.

In order to test the robustness of the proposed iteration scheme, numerical tests of the iterated chip thickness convergence are made for different starting values of inherent parameters. On one hand, offset values of the cutter center ($\delta_{x,i-1,j}$, $\delta_{y,i-1,j}$) in the precedent tooth path are initialized as a multiple of factor x ($x = 0$, 0.5, 1, 1.2, 1.5) times relative cutter/workpiece deflections that are calculated with nominal chip thickness. The iteration histories of the IUCT with different valves of x are plotted in Fig. 11a. Obviously, chip thickness converges unconditionally to the nominal value no matter what x is. On the other hand, the influence of parameter λ involved in Eq. 22 upon the IUCT convergence is also investigated. Iteration histories related to the IUCT of cutter element {1,35} are shown in Fig. 11b. Large values of λ are helpful to speed up the convergence.

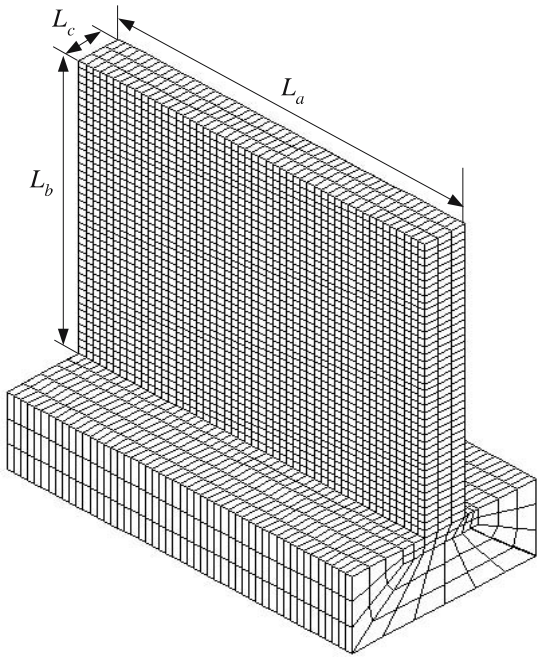

Fig. 8. Finite element model of the workpiece

Table 1. Cutting parameters

Cutting parameters	Test 1	Test 2	Test 3	Test 4
Cutting force model	Model 1	Model 1	Model 1	Model 2
[K_T (MPa), K_R, K_z]	[1938,0.693,0]	[990,0.52,0]	[$207\bar{h}^{-0.67}$, $1.39\bar{h}^{-0.043}$, 0]	-
[K_{Tc} (MPa), K_{Rc} (MPa), K_{zc} (MPa), K_{Te} (N/mm), K_{Re} (N/mm), K_{ze} (N/mm)]	-	-	-	[951.365, 262.597, 323.330, 11.115, 11.314, 1.105]
Milling model	Down	Up	Down	Down
Cutter diameter (mm)	20	19.05	19.05	20
Gauge length of cutter (mm)	54.41	55	55.6	55.6
N	55	70	66	60
Helix angle of cutter	30°	30°	30°	30°
Tooth number	1	4	1	4
(L_a, L_b, L_c) (mm)	(47.96,38.1,5.5)	(47.96,38.1,5.5)	(63.5,34,2.45)	(47.96,38.1,5.5)
Axial depth of cut (mm)	38.1	19	38.1	18
Radial depth of cut (mm)	1	2	0.65	5
Feed (mm/tooth)	0.05	0.14	0.008	0.1
Data source	Ref. [5]	Ref. [1]	Ref. [4]	Ref. [7]

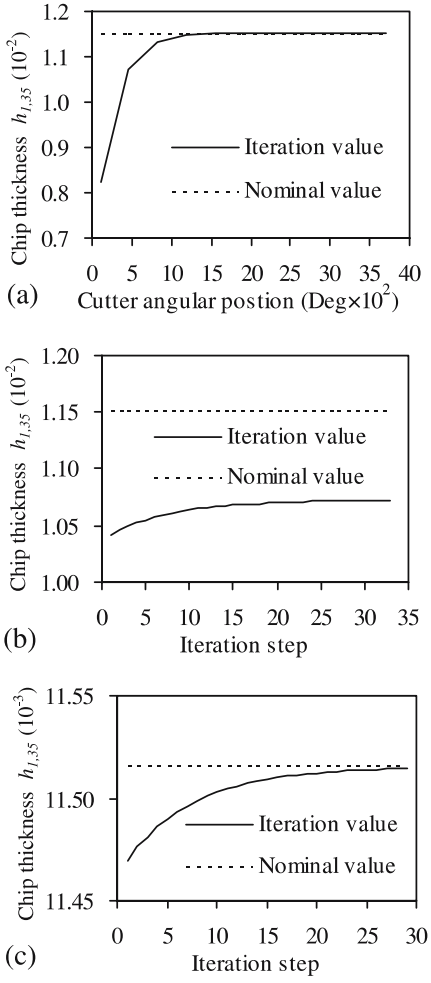

Fig. 9a–c. Test 1: Prediction of chip thickness $h_{1,35}$ with $\theta_{1,35} = 166.684°$ **a** Evolution of the chip thickness versus cutter angular position **b** Iteration history in the cutter angular position 462.857° **c** Iteration history in the cutter angular position 2622.857°

Test 2: It is now concerned with up milling. The cutting force model used is still Model 1. Resultant cutting forces between two curves named "Iteration value" and "Nominal value" are compared in Fig. 12a. Current results are also coherent with the referenced ones shown in Fig. 12b. Figure 13a plots the iteration history of the chip thickness related to cutter elements $\{i, 9\}$ versus cutter angular position during the milling process. It can be seen that the iteration value converges to the nominal value after several rotation angles. Besides, the sub-iteration history of the chip thickness in the 6th tooth period is shown in Fig. 13b, where the relative deviation between the iteration value and nominal one is less than 1% after the convergence is obtained. So, the cutting arrives at the steady state in this tooth period. From Figs. 12 and 13, it turns out that the regeneration phenomenon vanishes in a few tooth periods.

Test 3: This test deals with a more flexible workpiece with a smaller thickness of 2.45 mm in order to test the validity of the numerical approach. In Fig. 14a, evolution curves of the resultant cutting forces are plotted versus cutter angular position. Also,

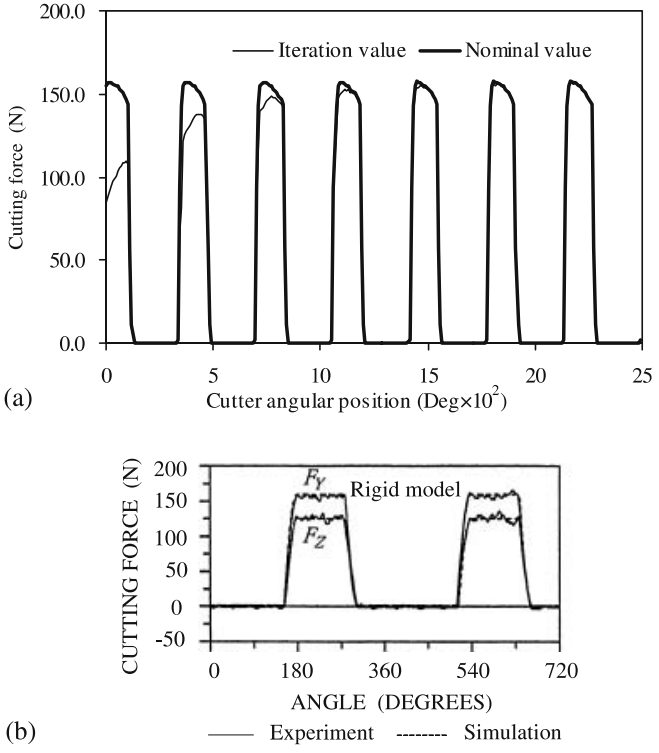

Fig. 10a,b. Test 1: Prediction of resultant cutting forces **a** Cutting force component F_Y **b** Referenced results from [5]

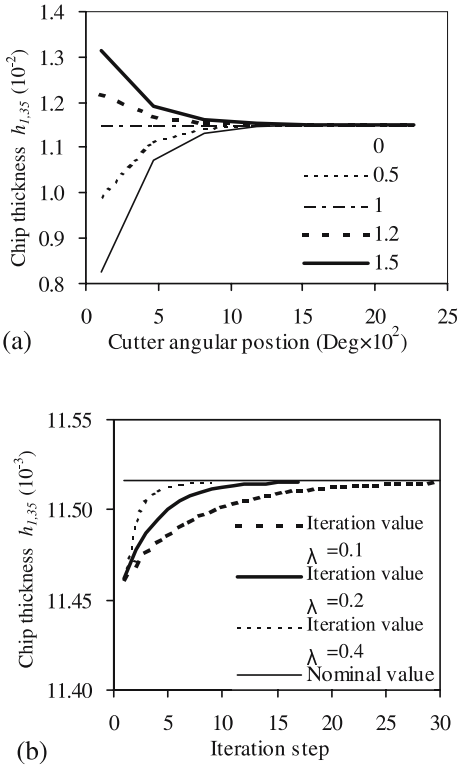

Fig. 11a,b. Test 1: The curves related to chip thickness iteration scheme with $\theta_{1,35} = 166.684°$ **a** Iteration histories with different initialized deflections **b** The influence of λ

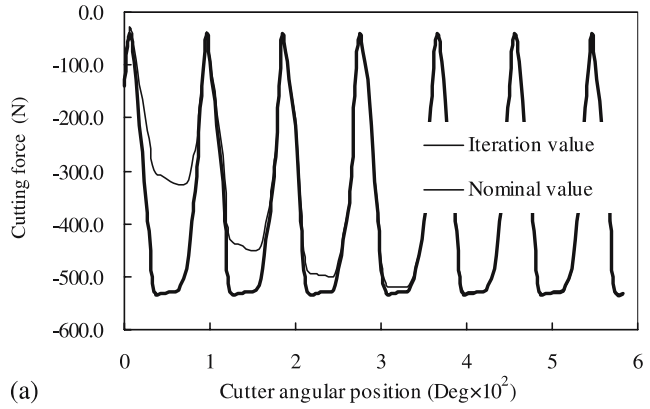

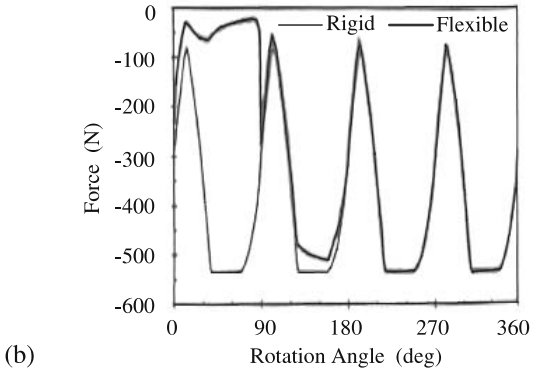

Fig. 12a,b. Test 2: Prediction of resultant cutting force **a** Cutting force component F_X **b** Referenced results from [1]

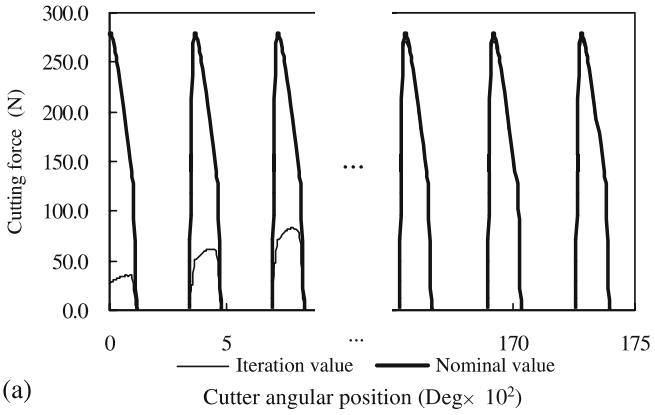

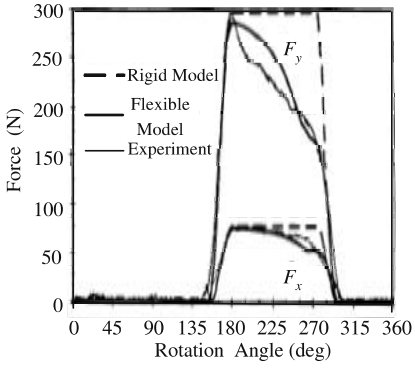

Fig. 14a,b. Test 3: Prediction of resultant cutting force **a** Cutting force component F_Y **b** Referenced results from [4]

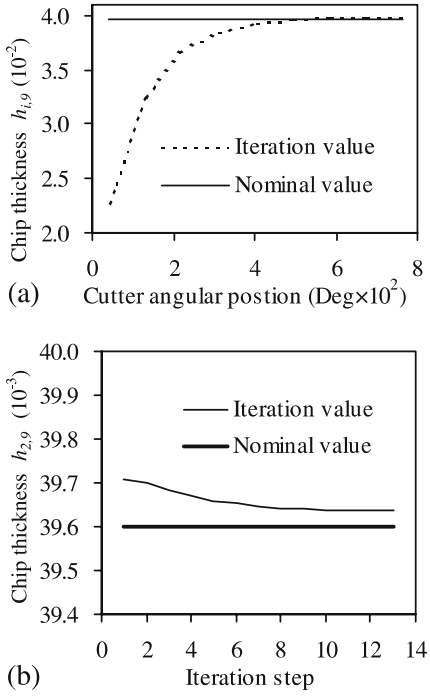

Fig. 13a,b. Test 2: Prediction of chip thickness $h_{i,9}$ with $\theta_{i,9} = 163.57°$ **a** Evolution history versus cutter angular position **b** Iteration history in the cutter angular position 492.353°

corresponding referenced results are shown in Fig. 14b for comparison. Figure 15 illustrates the iteration history of chip thickness. All these curves confirm that the regeneration mechanism is short lived and cutting forces can be well predicted by using nominal chip thickness. However, in this case, it can be seen that there exists a relatively slow convergence speed with respect to precedent tests due to the weaker rigidity of the workpiece.

Test 4: Model 2 is adopted as an alternative cutting force model for the considered workpiece in this test. The same numerical approach is applied to show its suitability. In Fig. 16a, resultant cutting force component F_Y is numerically predicted. It

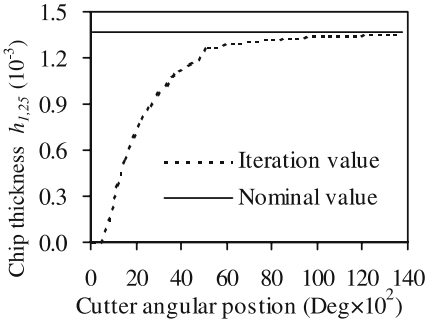

Fig. 15. Test 3: Evolution history of $h_{1,25}$ with $\theta_{1,25} = 170.195°$

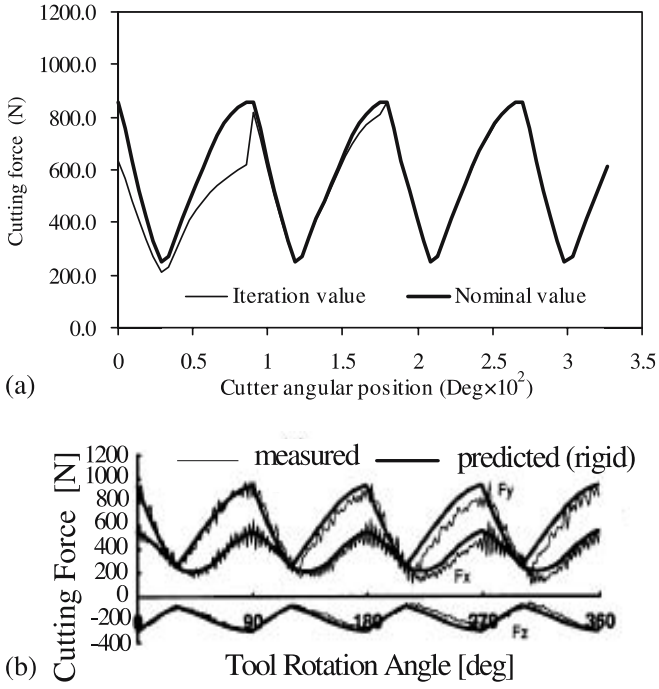

Fig. 16a,b. Test4: Prediction of resultant cutting forces **a** Cutting force component F_Y **b** Referenced results from [7]

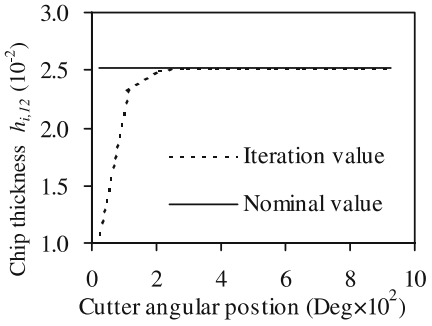

Fig. 17. Test 4: The general trend of $h_{i,12}$ with $\theta_{i,12} = 165.367°$

can be seen that the cutting force based on the iterated chip thickness is in good agreement with that using nominal chip thickness from the 4th tooth period. Meanwhile, compared with the experiment results given in Fig. 16b, a good coherence exists. Alternatively, the iteration history of the chip thickness associated with cutter elements $\{i, 12\}$ is also shown in Fig. 17. The iteration converges quickly. All results of this test show that the regeneration phenomenon still vanishes after some tooth intervals.

5 Conclusions

This paper investigates the numerical prediction of the chip thickness and the transient cutting forces in flexible end milling system using the finite element method. The cutter is modeled as a cantilevered beam, while the workpiece is discretized with free finite element meshes. The main work is focused on the derivation of instantaneous uncut chip thickness in terms of deflections, the establishment of iterative algorithms for chip thickness and radial depth of cut. With the proposed milling simulation procedure, abundant tests are numerically carried out and simulation results are validated by means of available experimental data. It is shown that in flexible static end milling, the regeneration mechanism is always short lived. Convergences of the radial depth of cut, the IUCT as well as cutting forces are stable and unconditionally ensured even though different initialized values of certain inherent parameters and two different cutting force models are employed. The nominal value of chip thickness can be directly applied to predict the cutting forces with safety for both down milling and up milling. Prospectively, the proposed iterative algorithm of chip thickness may be extended for the simulation of dynamic milling process in which the feed per tooth varies frequently. This issue needs to be investigated further.

Acknowledgement The authors would sincerely express their thanks to Dr. Erhan Budak for providing reference [1]. This work is supported by the Doctorate Creation Foundation of Northwestern Polytechnical University (Grant No. CX200411), the Natural Science Foundation of Shaanxi Province (Grant No. 2004$E_2$17) and the National Natural Science Foundation of China (Grant No. 50435020).

References

1. Budak E, Altintas Y (1992) Flexible milling force model for improved surface error predictions. In: Proceedings of Engineering System Design and Analysis, ASME, Istanbul, Turkey, 47(1):89–94
2. Sarhan A, Sayed R, Nassr AA, El-Zahry RM (2001) Interrelationships between cutting force variation and tool wear in end-milling. J Mater Proc Tech 109(3):229–235
3. Li XL, Guan XP (2004) Time-frequency-analysis-based minor cutting edge fracture detection during end milling. Mech Syst Signal Process 18(6):1485-1496
4. Budak E, Altintas Y (1995) Modeling and avoidance of static form errors in peripheral milling of plates. Int J Mach Tools Manuf 35(3):459–476
5. Tsai JS, Liao CL (1999) Finite-element modeling of static surface errors in the peripheral milling of thin-walled workpieces. J Mater Proc Tech 94(2–3):235–246
6. Wan M, Zhang WH, Qiu KP, Gao T, Yang YH (2005) Numerical prediction of static form errors in peripheral milling of thin-walled workpieces with irregular meshes. ASME J Manuf Sci Eng 127:13–22
7. Shirase K, Altintas Y (1996) Cutting force and dimensional surface error generation in peripheral milling with variable pitch helical end mills. Int J Mach Tools Manuf 36(5):567–584
8. Lee AC, Liu CS (1991) Analysis of chatter vibration in the end milling process. Int J Mach Tools Manuf 31(4):471–479
9. Semercigil SE, Chen LA (2002) Preliminary computations for chatter control in end milling. J Sound Vib 249(3):622–633
10. Kim SK, Lee S-Y (2001) Chatter prediction of end milling in a vertical machining center. J Sound Vib 241(4):567–586
11. Martellotti ME (1945) An analysis of the milling process. Part II: Down milling. Trans ASME 67:233–251
12. Koenigsberger F, Sabberwal AJP (1961) An investigation into the cutting force pulsations during milling operations. Int J Mach Tool Des Res 1:15–33
13. Kline WA, DeVor RE, Lindberg JR (1982) The prediction of cutting forces in end milling with application to cornering cuts. Int J Mach Tool Des Res 22(1):7–22
14. Altintas Y, Spence A (1991) End milling force algorithms for CAD systems. CIRP Ann 40(1):31–34

15. Budak E, Altintas Y, Armarego EJA (1996) Prediction of milling force coefficients from orthogonal cutting data. ASME J Manuf Sci Eng 118:216–224
16. Zheng CM, Wang J-JJ (2003) Estimation of in-process cutting constants in ball-end milling. Proc Inst Mech Eng, Part B: J Eng Manuf 217:45–56
17. Armarego EJA, Deshpande NP (1991) Computerized end-milling force predictions with cutting models allowing eccentricity and cutter deflections. CIRP Ann 40:25–29
18. Yücesan G, Altintas Y (1994) Improved modeling of cutting force coefficients in peripheral milling. Int J Mach Tools Manuf 34(4):473–487
19. Sutherland JW, DeVor RE (1986) An improved method for cutting force and surface error prediction in flexible end milling systems. ASME J Eng Ind 108:269–279
20. Kline WA, DeVor RE (1983) The effect of runout on cutting geometry and forces in end milling. Int J Mach Tool Des Res 23(2–3):123–140
21. Smith S, Tlusty J (1991) An overview of modeling and simulation of the milling process. ASME J Eng Ind 113(2):169–175